A Novel Complimentary Filter for Tracking Hip Angles During Cycling Using Wireless Inertial Sensors and Dynamic Acceleration Estimation

John Cockcroft, Jacobus H. Muller, and Corie Scheffer, *Member, IEEE*

***Abstract*— As wireless motion sensors become more compact and robust, new opportunities emerge to develop wearable measurement technologies for in-field sports analysis. This paper presents a nonlinear complimentary filter for tracking 3-D hip joint angles during cycling using inertial and magnetic measurement systems (IMMSs). The filter utilizes a novel method of dynamic acceleration compensation in the sensor frame based on the assumption of pendulum motion of the thigh around the hip joint center. A dynamic calibration is proposed in which the center of rotation of the thigh IMMS can be estimated during a functional hip movement in standing. Validation results from a gold-standard optical system showed that the filter IMMS tracking is drift-free with mean absolute errors of less than 3° for all IMMS axes combined at low, medium, and high pedaling speeds. Hip angles were also validated using the Vicon biomechanical model for standing and sitting calibration poses as well as true and normalized soft-tissue-artefact (STA). The best mean absolute errors for the sagittal, frontal, and coronal planes were 0.8°, 6.7°, and 2.2°, respectively. Variability due to calibrations and STA ranged from 1.4° to 8.1°. This demonstrates the high accuracies possible for IMMS tracking using algorithms designed for specific sports despite larger errors due to modeling.**

***Index Terms*— Wireless motion capture, inertial and magnetic sensing, complimentary filtering, dynamic acceleration compensation, human movement, sports biomechanics.**

I. Introduction

IN THE past, sports biomechanics research has been conducted using laboratory-based measurement technologies. Inevitably, the ecological validity of findings in these controlled environments has been debated [1]–[3]. However, the development of compact wearable sensors is now enabling in-field biomechanical analysis for a growing number of sports [4], [5]. An example of this is inertial and magnetic measurement systems (IMMSs), small wireless sensor units containing orthogonal triads of accelerometers, gyroscopes and magnetometers [6]. IMMSs have the key advantage of tracking their own orientation proprioceptively without the external infrastructure required by other motion capture systems [7], [8]. This enables outdoor tracking of 3D body segment orientation and multi-segment outputs such as joint angles using biomechanical modeling techniques [9]. However, despite utilization in a number of human movement applications such as pedestrian tracking [10], clinical gait analysis [11], activity monitoring [12] and rehabilitation [13], the full-scale adoption of IMMSs in sports biomechanics is hindered by a lack of accuracy in joint angle estimation.

IMMS joint angle estimation is a two-step process: tracking the IMMSs attached to the body and then transforming IMMS orientations to an anatomical coordinate frame (ACF) defined for each segment. Therefore, the two primary sources of error in IMMS joint angle estimation are misalignment of IMMSs in relation to their segment ACFs, and error in IMMS tracking. IMMSs are unable to directly measure ACF orientation, necessitating calibrations in which the IMMS-to-segment orientation is estimated from a static pose with known ACF orientations [9]. Although further dynamic calibrations can then be implemented for correcting knee joint axis misalignment, a weakness of IMMS joint angle estimation is that the orientation of the pelvis is unknown during calibration, directly affecting the reliability of hip joint output. Moreover, variable and transient misalignment can occur due to the well-known effects of soft-tissue-artefact (STA).

A variety of algorithms exist for IMMS tracking, all of which 'blend' two measurements of the IMMS orientation. The first type of measurement is gyroscope tracking, using strapdown integration methods, which provides excellent high frequency motion registration. However, it suffers from well-known drift and quantization errors and requires external initialization due to a lack of absolute measurements [14]. In the second method, accelerometers and magnetometers track orientation by sensing Earth's gravitational and magnetic fields, respectively, using static frame vector-matching techniques. Conversely, this provides absolute measurements with good accuracy at low frequencies but high levels of noise during rapid motion or magnetic interferences [15]. Therefore, all IMMSs utilize some form of mathematical sensor fusion to exploit these complementary measurement features.

Crassidis et al. [16] provide a comprehensive survey of research developments in the area of orientation tracking algorithms. The traditional 'workhorse' for optimal IMMS sensor fusion is the extended Kalman filter (EKF) which has performed well in many applications. However, the EKF has known limitations, most significantly its basis upon a linearization of the system. Efforts to overcome this have led to the development of more sophisticated statistical optimization methods such as unscented Kalman and particle

Manuscript received February 13, 2014; revised April 9, 2014; accepted April 9, 2014. Date of publication April 29, 2014; date of current version July 1, 2014. The associate editor coordinating the review of this paper and approving it for publication was Prof. Elena Gaura.

The authors are with the Department of Mechanical and Mechatronic Engineering, Stellenbosch University, Stellenbosch 7600, South Africa (e-mail: johnc@sun.ac.za; cscheffer@sun.ac.za; cobusmul@sun.ac.za).

Color versions of one or more of the figures in this paper are available online at http://ieeexplore.ieee.org.

Digital Object Identifier 10.1109/JSEN.2014.2318897

filters. Secondly, the large covariance matrices of an EKF make it notoriously difficult to tune [17]. From early years this drove the utilization of simpler deterministic complimentary filters that require the tuning of only one or two scalar gains [18]. More recently, more robust non-linear complementary filters have been developed for UAV tracking [19] that have shown comparable performance to the EKF. Non-linear observers have the desirable feature of being asymptotically stable, i.e. converging from any initial condition [20].

Other developments in IMMS tracking have focused on the incorporation of prior knowledge about the system [14]. For example, non-holomic constraints such as zero lateral velocity have also been successfully implemented in ground vehicle tracking [21], [22]. In pedestrian tracking using foot-mounted IMMSs, updates for zero velocity, zero-attitude and zero-integrated heading rate during strategic points in a movement have also yielded improvements to tracking accuracy [10]. In multi-IMMS body-networks, holonomic constraints on the degrees of freedom in an anatomical joint of the body model can reduce orientation errors [23]. Without aiding sensors such as Global Positioning Systems (GPS), a crucial aspect of IMMS tracking is compensation for dynamic accelerations which otherwise corrupt gravity estimates and cause drift errors. While basic methods employ time-averaging in the sensor coordinate frame [24], this is susceptible to bias errors due to centripetal accelerations [25]. To the authors' best knowledge there is only one published method for centripetal acceleration compensation in the sensor frame, which is only relevant to UAV flight with a wind-speed sensor [26]. The majority of published methods are based on the assumption of zero-mean accelerations in the global frame [27], [28], although researchers have commented on the scarcity of details for these methods in scientific literature [29].

One sport which stands to benefit from IMMS technology is road cycling, where outdoor measurements could better inform efforts to improve biomechanical efficiency and minimize injury risk. However, there are also challenges. The movement is sustained over long periods of time and exhibits large and continuous centripetal accelerations, both of which lead to drift errors. The margins for improvement in body position are also small, requiring high accuracy. The feasibility of testing cycling using IMMSs has already been demonstrated with a proprietary tracking algorithm [30], [31]. The authors could find only one published algorithm designed for cycling in which a gyroscope reset method was used to track joint kinematics with no drift [32]. However, the study in [32] was limited. It was conducted with 2D sensors, accelerometers were not used for inclination sensing and the results excluded hip angles. The aim of this study was to develop a method for measuring hip angles in cycling which combines the measurement capabilities of IMMSs with the power and simplicity of non-linear complimentary filtering.

II. Methods

A. Experiments

One subject was tested pedaling on a competition standard road bicycle attached to a stationary trainer in an indoor laboratory. The subject was instructed to cycle for three consecutive 5-minute periods at a self-selected slow (measured cadence $\approx$ 45 rpm), medium ($\approx$ 65 rpm) and fast ($\approx$ 85 rpm) pedaling speed respectively. Pelvis and thigh segment kinematics were measured using wireless IMMSs developed by Xsens (MTw Development Kit, B.V. Technologies, Enschede, Netherlands). The pelvis IMMS was attached to the sacrum and the left and right thigh IMMSs were fixed on the distal third on the line between the greater trochanter and the lateral epicondyle of the knee. To limit magnetic interference, the testing was conducted in a magnetically clean location according to recommendations proposed by Veeger et.al [33].

To validate the IMMS filter results, the orientation of each IMMS was also tracked using a gold-standard optical motion capture system (Vicon MX, Oxford Metrics Group, Oxford). Three passive-reflective markers were attached to a rigid L-shaped plastic cluster which was tightly taped to the casing of each IMMS. The cluster markers were then used to reconstruct the IMMS orientation in the Vicon laboratory frame according to the method proposed by Veeger et.al [33]. Pelvis and thigh segment markers were also placed on the subject according to the instructions for the standard Vicon Plug-in-Gait biomechanical model. The hip joint angle output from the model was used as a ground-truth reference to validate the hip angles calculated using the IMMSs. Model calibrations for both systems were performed using a static T-pose. During the three speed trials the data from the IMMSs and Vicon were collected synchronously at 75 Hz using the coaxial cables, ports and settings prescribed in the Xsens documentation.

B. Filter Design

This study involved the adaptation of a passive complementary filter (PCF) from the class of deterministic non-linear observers proposed by Mahoney [20]. The output from the PCF is an estimate of the IMMS orientation q with respect to a north-east-up global frame, represented by the quaternion parameterization in Hamilton notation with

$$\hat{q} = [\hat{s} \quad \hat{\boldsymbol{v}}] \tag{1}$$

where s is the scalar component, $\boldsymbol{v}$ is a three-element vector and the accent symbol $\hat{q}$ represents an estimate of the true quantity q. The filter receives 3D measurement inputs from a gyroscope, accelerometer and magnetometer designated y_G, y_A and y_M respectively. The sensor models for each were:

$$y_G(t) = \omega^S(t) + b^S(t) \tag{2}$$

$$y_A(t) = a^S(t) - g^S(t) \tag{3}$$

$$y_M(t) = m^S(t) + d^S(t) \tag{4}$$

Here ω^S, a^S, g^S and m^S are 3D vectors representing angular velocity, dynamic and gravitational accelerations and magnetic field intensity respectively. The gyroscope signal contains a bias b^S and the magnetometer signal contains magnetic field disturbances d^S. All terms are expressed in the sensor frame, designated by superscript S The relationship between q and ω is governed by the following differential equation for rigid

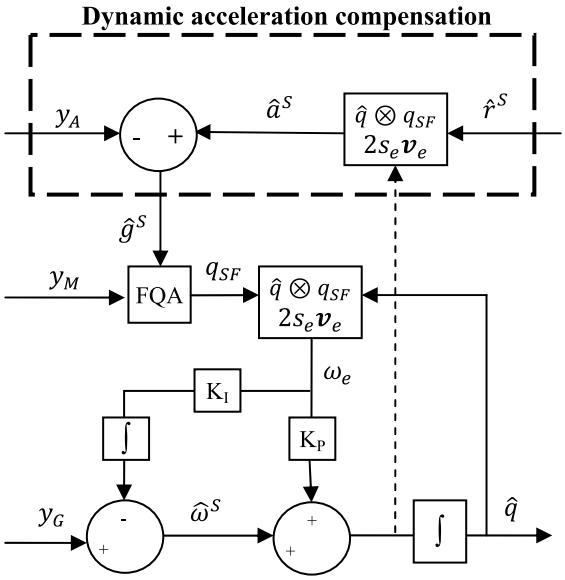

Fig. 1. Block diagram of the Pendulum Filter with DAC.

body kinematics:

$$\dot{\hat{q}} = \frac{1}{2} q \otimes p(\widehat{\omega}) \tag{5}$$

The symbol $\otimes$ in (5) refers to a quaternion multiplication and the pure quaternion form of ω is $p(\omega) = \begin{bmatrix} 0 & \omega \end{bmatrix}$. The filter thus needs to estimate ω from (2) and use it to integrate (5) to track q from an initial condition q_0. This is done by compensating for b^S in (2) using (3-4). The basic structure of the PCF is given below. Details can be found in [20].

$$q_e = \hat{q} \otimes q_{SF} = \begin{bmatrix} s_e & \boldsymbol{v}_e \end{bmatrix} \tag{6}$$

$$\omega_e = 2 s_e \boldsymbol{v}_e \tag{7}$$

$$\dot{\hat{b}} = -K_I \omega_e \tag{8}$$

$$\widehat{\omega} = y_G - \hat{b} + K_P \omega_e \tag{9}$$

Fig. 1 gives a summary of the adapted PCF, hereafter named the Pendulum Filter since it is based on the assumption of pendulum motion for the thigh IMMS. The PCF estimates $\widehat{\omega}$ according to equations (5-9). The filter performs online bias correction in (8) using an integrator and incorporates a feedback ω_e: the error between the last estimate $\hat{q}$ error and the orientation q_{SF} reconstructed with the accelerometer and magnetometer. The Factored Quaternion Algorithm (FQA) was chosen to calculate q_{SF} for this study as, unlike other methods, it decouples the effects of magnetic interference from the inclination angles [34]. The dynamic acceleration compensation method in Fig. 1 is described next in Section C.

The filter gain K_I was set at a value twenty times smaller than the proportional gain K_P, which was optimized for the slow, medium and fast trials individually. The optimization was conducted by running the filter through a 1D grid search of K_P between the extreme values of 0 (gyroscope tracking only) and 5 (effectively FQA only). The optimum gain value was chosen as the value resulting in the lowest combined minimum mean absolute error (CMAE) for all three axes. Thigh IMMS

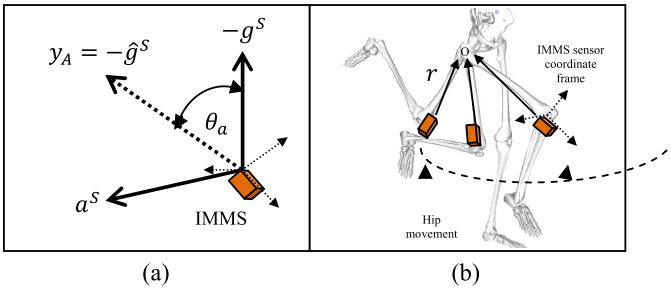

Fig. 2. The (a) errors in gravity tracking without DAC and (b) the calibration hip movement (sagittal plane view).

tracking and gain optimization was implemented for both the Pendulum Filter as well as the basic PCF without dynamic acceleration compensation (DAC), to allow for comparison, while only the PCF filter was used for the pelvis IMMS.

C. Dynamic Acceleration Compensation

One of the limitations of Mahoney's PCF in [20] is that it assumes that the dynamic acceleration in the sensor frame is both weak ($a^S \ll g^S$) and zero-mean. However, neither assumption holds for cycling where leg segments experience significant centripetal accelerations. In this study, the centripetal accelerations were sinusoidal with peaks of approximately $0.2g$, $0.6g$ and $1g$ for the slow, medium and fast pedaling speeds respectively. Separate tests showed that during sprinting cadences, a^S could exceed $3g$. Without DAC, a^S in (3) acts as noise which severely corrupts the accelerometer's estimate of gravity in (3). As illustrated in Fig. 2a, the uncompensated accelerometer estimate of $-\hat{g}^S$ (used as the vertical direction of the IMMS reference frame) causes an IMMS inclination error θ_a in q_{SF} proportional to the magnitude and direction of a^S. Estimation of a^S using a DAC method is thus highly desirable for improving orientation estimates. Fig. 1 illustrates how the Pendulum Filter compensates for dynamic accelerations in the accelerometer signal in order to produce a better gravity estimate $\hat{g}^S$. By including a priori information, namely the assumption of pendulum motion for the thigh segment, the acceleration of the thigh IMMS can be expressed in terms of the acceleration of the centre-of-rotation (CoR) a_O and the radial and tangential accelerations a_r and a_t as in (10). By assuming that a_O^S is negligible for the pelvis during cycling, (10) can be rewritten in terms of the angular velocity of the thigh and the CoR of the IMMS r^S as in (11).

$$a^S(t) = a_O{}^S(t) + a_r{}^S(t) + a_t{}^S(t) \tag{10}$$

$$= \frac{\mathrm{d}\omega^S}{\mathrm{dt}} \times r^S + \omega^S \times (\omega^S \times r^S) \tag{11}$$

Since the estimate $\widehat{\omega}^S$ can be obtained from the PCF all that is required to make an estimate for a^S is an estimate of $\hat{r}^S$:

$$\hat{a}^S = \frac{\mathrm{d}\widehat{\omega}^S}{\mathrm{dt}} \times \hat{r}^S + \widehat{\omega}^S \times (\widehat{\omega}^S \times \hat{r}^S) \tag{12}$$

The vector $\hat{r}^S$ was estimated in this study using a simple calibration procedure in which the subject, after standing still

TABLE I
OPTIMAL FILTER GAINS

Filter	Slow	Medium	Fast
Passive	0.2	0.17	0.14
Pendulum	0.5	0.4	0.3

for 3 seconds in a single leg standing position, performed a repeated hip joint excursion for 5 seconds (see Fig. 2b).

The key to the calibration is that it is also possible to track a^S by rearranging (12) into the form of (13). It is then possible to estimate the gravity vector g^S in (13) using (14).

$$a_{cal}{}^S = y_A + \hat{g}^S \tag{13}$$

$$p(\hat{g}^S) = \hat{q}^* \otimes p(\hat{g}^G) \otimes \hat{q} \tag{14}$$

Here, $\hat{q}^*$ is a conjugated quaternion. Since the accelerometer signal y_A and the gravity vector in the global frame g^G in (13) are known, all that is needed to calculate $\hat{r}^S$ in (12) is the orientation $\hat{q}$ of the sensor during the movement in (14). Due to the short duration of the calibration, $\hat{q}$ can be estimated with sufficient accuracy by solving (5) using the orientation at standstill q_0 (calculated using FQA) and substituting y_G for ω. Thus, using gyroscope integration $a_{cal}{}^S$ was tracked in (13-14) and used to solve for $\hat{r}^S$ in (12). Furthermore, due to sensor noise a least squares algorithm was employed to optimize $\hat{r}^S$. In this study, a global grid search was employed to find the three elements of $\hat{r}^S$, and a MAE cost function E was chosen to be minimized as in (15).

$$E = \sum^t \left\| a_{cal}{}^S(t) - \hat{a}^S(t) \right\| \tag{15}$$

It should be noted that a_R^S is highly corrupted by high frequency noise due to the numerical differentiation of ω^S in (10). Various filtering methods were attempted to attenuate the noise, and eventually a low-pass 4$^{\text{th}}$-order Butterworth filter with a cut-off frequency of 15 Hz was chosen to smooth a_R^S.

D. Data Analysis

The optimum gain values for the PCF and Pendulum Filters are given in Table I. As expected, the optimal filter gain values decrease with increasing dynamic acceleration. It is clear from the higher Pendulum Filter gains that the Pendulum Filter weights q_{SF} more heavily and is thus more resilient to dynamic accelerations.

To compare Vicon measurements of $\hat{q}$ with the IMMS results it was necessary to align the reference frames for the two systems. The quaternion $q_{I\to L}$, representing the transformation between the laboratory and the IMMS frames, was obtained after a five minute stationary period using the average orientation output of the Xsens Kalman filter over one minute (assuming zero-mean static error).

$$q_{I\to L} = q^*{}_{cluster} \otimes q_{kalman} \tag{16}$$

The Vicon marker trajectories were high pass filtered using the Vicon Woltring filter routine with an MSE of 20mm. Hip joint angles were defined, according to the Plug-in-Gait model conventions, as the orientation of the anatomical coordinate frame (ACF) of the distal femur relative to the ACF of the pelvis. Unlike in optical motion capture where the ACFs are defined by markers placed on anatomical landmarks, IMMS are unable to directly measure in the ACFs. IMMS-to-segment orientation $q_{S\to B}$ was calculated during a static pose calibration from q_S and an ACF orientation $q_{\mathbf{B}}$:

$$q_{S\to B} = q^*{}_B \otimes q_S \tag{17}$$

Rather than assume the calibration values for q_B, both the pelvis and thigh segments $q_{S\to B}$ values were calculated using the Vicon Plug-in-Gait ACF orientations during two static trials: one standing in a T-pose position and the other sitting upright on the bike with the crank arm held in a horizontal position. The hip joint angles were then calculated using

$$q_B = q_S \otimes q^*{}_{S\to B} \tag{18}$$

Furthermore, hip joint angles were also calculated using the Vicon marker trajectories and the Plug-in-Gait model in two ways. The first was the standard method of using the markers placed on the skin. The second involved the virtual reconstruction of the skin marker positions based on their relationship to the Vicon coordinate system attached to the segment IMMS. This allows for a more direct comparison between the filter tracking results by ensuring that the STA is the same for both systems. Hip joint angles were calculated in Euler angles for intuitive interpretation.

III. RESULTS

A. Sensor Orientation Tracking

The accuracy of the PCF, Pendulum Filter and Xsens filter, defined as the combined MAE for all three axes (CMAE), is presented in Fig. 3 for the slow, medium and fast trials. It should be noted that the Pendulum Filter is only applicable to the thigh IMMS since the pelvis IMMS does not fulfill the assumption of pendulum motion. It can be seen from Fig. 3a that the PCF performed very well in all three speed conditions for the pelvis IMMS, with CMAEs of 2.8°, 2.7° and 2.5° for slow, medium and fast pedaling. The Xsens filter performed within the MTw accuracy specifications with CMAEs of 2.7°, 2.6° and 1.9°. Fig. 3(b) shows the average of the left and right thigh IMMS CMAEs. The PCF performed relatively well during slow pedaling (CMAE = 4.3°), with the errors then more than doubling for medium pedaling speed (CMAE = 9.4°) and then more than doubling again for the fast trial (CMAE = 19.8°). The Pendulum Filter in Fig 3(b), on the other hand, notably outperformed the PCF with CMAEs of 2.1°, 2.6° and 2.6° for the three trials respectively. This was only marginally higher than the Xsens filter, which produced CMAEs of 2.1°, 2.1° and 1.8° for slow, medium and fast pedaling. This equates to an average MAE $< 1°$ for individual IMMS axes, which is very low and approaching the accuracy thresholds of both the IMMSs and Vicon validation method due to white noise.

B. Hip Joint Angle Tracking

Since the Pendulum Filter accuracy was consistent across a range of dynamics, the effect of pedaling rate on hip joint

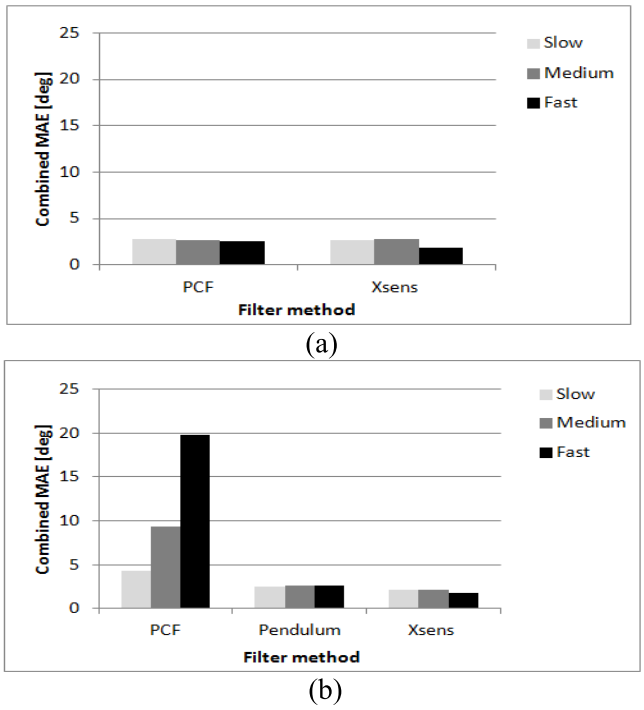

Fig. 3. Comparison of filter performances at different pedaling speeds for the (a) pelvis and (b) thigh IMMSs.

angle accuracy was assumed negligible. Therefore, for the sake of brevity, the hip joint angles for the sagittal, frontal and coronal planes are only reported here for the fast pedaling trial (worst STA scenario). The hip angles were calculated with and without skin marker STA for the Vicon model, and using the sitting and standing segment calibrations for the IMMSs.

Fig. 4 shows hip joint angle curves for a representative pedal revolution chosen in the last minute of the trial. This allows for a visual illustration of the various factors affecting the accuracy of the results. The difference between the IMMS results (shown in grey in Fig. 4), which are calculated using the same sensor orientations, is predominantly influenced by the differences in STA during sitting and standing calibrations. This is attested by the constant offset between the curves. The dissimilarity between the two Vicon results (shown in black in Fig. 4), on the other hand, is a result of the different STA effects local to the IMMS sensor (No STA condition) and the Vicon skin markers (STA condition). As would be expected, these manifest in more variable curve deformations due to differences in STA local to the IMMS and skin markers. Interestingly, the effects of skin marker STA are more pronounced near the bottom of the pedal stroke (minimum hip flexion), likely due to muscle contractions and movement of the ilio-tibial band when the leg is near full extension.

Besides the effect of calibration pose on IMMS results and that of STA on the Vicon results, comparisons can also be made between Vicon and IMMS hip angle outputs. Quite clearly, the sitting calibration is more accurate (similar to the Vicon outputs) in comparison to the standing calibration, as evidenced by the solid grey curve being closer to the black curves. Intuitively, the No STA curve shapes are also more

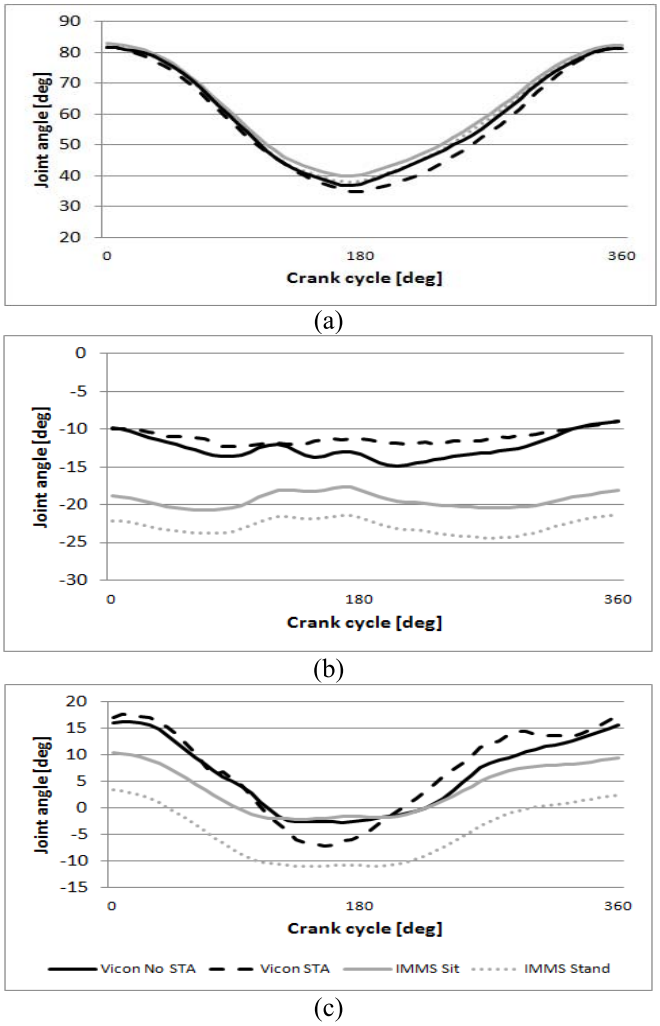

Fig. 4. Representative hip (a) sagittal plane flexion, (b) frontal plane abduction and (c) coronal plane rotation angles (internal rotations positive) for a crank cycle.

similar to the IMMS shapes than the STA curves as they share a common STA locality on the IMMS. Nevertheless, a true comparison of the Vicon and IMMS systems would be between the IMMS standing and Vicon STA data. In addition to the comparison of Vicon and IMMS data, it is also of interest to investigate the effects of errors on the three different planes of motion of the hip.

The dominant hip motion during cycling is flexion in the sagittal plane, demonstrated by the large hip flexion range of motion ($>40°$). Interestingly, however, hip flexion shows the least variation due to calibration pose amongst the three planes, which can be seen by the similarities in shape. Differences in absolute values, in contrast, are not clear from Fig. 4 due to axis scaling. To provide more detail on shape and absolute errors, Tables II and III give the squared correlation coefficients and MAEs between all four conditions. The R^2 and MAE values in Tables II and III can be used to compare the proportion of the errors due to STA on the Vicon alone (top left block for each plane), to IMMSs calibrations alone (bottom left block), to STA between the systems (top to bottom of four top right blocks) and calibration between the systems (left to right). The analysis confirms that the IMMS hip flexion

TABLE II
HIP ANGLE SQUARED CORRELATION COEFFICIENTS

	VICON		IMMS	
	No STA	**STA**	**Sit**	**Stand**
SAGITTAL PLANE (R^2)				
Vicon No STA		0.9832	0.9981	0.9980
Vicon STA			0.9875	0.9873
IMMS Sit				1.0000
IMMS Stand				
FRONTAL PLANE (R^2)				
Vicon No STA		0.9168	0.6054	0.6315
Vicon STA			0.7203	0.7287
IMMS Sit				0.9710
IMMS Stand				
CORONAL PLANE (R^2)				
Vicon No STA		0.9539	0.9542	0.9605
Vicon STA			0.9703	0.9724
IMMS Sit				0.9984
IMMS Stand				

TABLE III
HIP ANGLE MAES

	VICON		IMMS	
	No STA	**STA**	**Sit**	**Stand**
SAGITTAL PLANE (deg)				
Vicon No STA		2.1	2.2	0.8
Vicon STA			3.6	2.4
IMMS Sit				1.4
IMMS Stand				
FRONTAL PLANE (deg)				
Vicon No STA		1.2	6.9	10.5
Vicon STA			8.0	11.6
IMMS Sit				3.6
IMMS Stand				
CORONAL PLANE (deg)				
Vicon No STA		2.9	2.2	9.9
Vicon STA			4.7	11.3
IMMS Sit				8.1
IMMS Stand				

tracking was especially accurate compared to the Vicon STA results (all $R^2 > 0.98$ and MAE $< 4°$).

As expected, the frontal and coronal plane tracking was less accurate than for the sagittal plane. CMAEs for both planes were over 10° for standing IMMS. However, both also showed improved MAEs when STA was made common and a sitting calibration was used. These improvements were cumulative, resulting in a reduction in both the frontal (MAE = 6.9°) and coronal (MAE = 2.2°) planes.

Interestingly, while all coronal plane curve shapes were very similar ($R^2 > 0.95$), correlations were only moderate in the frontal plane between systems (0.6 - 0.73). Nevertheless, intra-system comparisons for the Vicon ($R^2 \approx 0.91$) and IMMS ($R^2 \approx 0.97$) and small inter-system differences suggest that the lower inter-system values are due to factors other than STA or calibration. These factors remain unclear, but may be related to non-linear effects introduced by the Vicon Plug-in-Gait model's definition of the femur. Unlike the IMMS system, Vicon femur orientation is tracked using hip centers estimated from the pelvis skin marker positions. Another plausible reason is that the frontal plane hip range of motion is relatively small compared to errors between systems.

IV. DISCUSSION

This study successfully implemented the two key features required for tracking 3D hip joint angles during cycling using IMMSs: IMMS tracking using complimentary filtering and IMMS-to-segment calibrations using an optical motion capture system. Overall the results confirm a significant improvement in IMMS tracking using a novel adaptation to the PCF. The results also serve to validate the wireless MTw IMMS from Xsens, which performed within specifications. Furthermore, the study reports good accuracy in hip angle tracking compared to a gold-standard optical system. Another study comparing Vicon joint angles to the Xsens biomechanical model outputs found similar results, with sagittal plane values being highly correlated and transverse and coronal plane angles being mildly correlated [35]. The analysis investigated the intra- and inter-system differences in hip angle outputs for all three anatomical joint planes of motion due to STA and calibration poses. One key finding was that the intra-system variability due to STA and calibration was in the same order of magnitude as the inter-system variability.

The IMMS tracking results highlight the influence of movement dynamics on filter performance when there is no DAC. Predictably, due to the low intensity of pelvis movement during cycling, the PCF performed very well for this segment at all speeds as well as for the thigh in the low pedaling speed trial. However, the medium and fast speeds violate the PCF's 'weak acceleration' assumption for the thigh IMMSs leading to large tracking errors. The Pendulum Filter tracking errors, on the other hand, were low and independent of pedaling dynamics. This demonstrates the efficacy of the CoR estimates from the dynamic calibration and the robustness of the DAC method. Moreover, with performance comparable to the advanced Xsens Extended Kalman filter, the Pendulum Filter supports claims that CFs can be implemented as successfully as EKFs [26].

Despite good IMMS tracking accuracy, the hip angle results demonstrate that the impact of segment calibration and STA on joint kinematics accuracy can be almost an order of magnitude larger than IMMS tracking errors. As is the case with most motion capture applications, the sagittal plane results were the most robust to changes in calibration and STA, with negligible differences between systems. The errors in the other two planes, however, were both over 10° for the standing calibration pose, which is significant, although the curves display very similar shapes. The reduction in error using the sitting calibration pose suggests that the sensor to segment

relationship changed between sitting and standing. This suggests, intuitively, that large STA errors may be introduced when the calibration pose is different to the movement pose - this is another noteworthy emphasis of the study. While the true effect of STA cannot be known either for Vicon or IMMS tracking without another gold-standard measurement (such as fluoroscopy), the results indicate that the STA for the two different systems was not significantly different in terms of CMAE. However, the shape of the graphs for the Vicon skin markers was different to the STA compensated Vicon outputs. This suggests that the sensor-to-segment orientation changed dynamically during the pendulum motion, changing the shape while still possibly maintaining a low MAE. This may affect the accuracy of analysis using variables such as range of motion.

The main contribution made by this study is that it describes a novel DAC method which is performed in the sensor frame, in contrast to the usual inertial frame approaches. The system utilizes a simple complimentary filter structure which demonstrates that more complex Kalman filtering is not always necessary to achieve good results. The novel calibration method for finding the CoR is also an addition to other methods used to estimate joint centres in the upper limbs [36]–[38]. Clearly, the CoR for the thigh segment can add valuable information about segment inclination which might be exploited in any filtering algorithm and perhaps for other human movements besides cycling, such as walking and running. However, the Pendulum Filter works best when the hip joint centre acceleration $a_O{}^S(t)$ in equation 10 is either negligible or known. In movements where the pelvis translates and $a_O{}^S(t)$ is not negligible it can still be estimated and compensated for if the pelvic orientation is accurately measured and gravity is removed. The CoR can also be estimated using a quick and simple dynamic calibration protocol that does not require any other instrumentation, making it suitable to implement in most testing conditions. The study also presents hip angle tracking for cycling using IMMS, which is currently sparse in the literature. The challenge of IMMS sensor-to-segment calibration is also highlighted, especially for the pelvis.

Nevertheless, the study has several limitations. Firstly, the IMMSs used were of a high quality, meaning that the sensor outputs are corrupted with less measurement noise and thus subject to less drift error than genuine low-cost IMMSs. However, informal gyroscope integration tests revealed that drift error for the Xsens IMMSs is still large after more than 30 seconds. Even so, work with less expensive IMMSs would necessitate retuning of the filter gains and may result in different levels of accuracy. Secondly, further testing should be conducted with more subjects, on different bicycles and at higher speeds (>100 rmp) to determine the sensitivity of the tracking accuracy to different levels of STA, movement and magnetic interference due to ferrous components. Furthermore, since the testing was performed indoors to facilitate the Vicon validation, the testing conditions excluded bicycle dynamics on the road. Further work thus needs to be done to understand the effects of accelerations due to a moving bicycle, which would require outdoor testing.

There is a clear need for developing innovative IMMS segment calibration methods which take the pose of the movement into account in order to reduce STA as well as modeling errors. The inherent limitations of static calibrations in which the segment pose is assumed could perhaps be overcome by the use of aiding technologies such as portable cameras, which could be used to provide segment poses on site similarly to the use of the Vicon in this study. It may also be beneficial to explore the optimization of IMMS placement to reduce both STA and accelerations due the CoR length.

V. Conclusion

This study presents a non-linear complementary filter with a novel DAC method applicable to tracking the orientation of an IMMS attached to the thigh during cycling. This method is based upon the assumption of pendulum motion for the thigh segment and was shown to drastically improve IMMS tracking for the same filter, especially with increasing pedaling cadences. Furthermore, while the DAC method is implemented in the sensor frame, it has very similar performance to the proprietary and industry-leading Xsens DAC method implemented in the inertial frame. The tracking of IMMSs on the pelvis and thigh of a cyclist allows for the calculation of useful biomechanical variables such as hip joint angles. Validation results proved that the IMMS hip joint outputs were highly accurate in the sagittal plane, and moderately so in the frontal and transverse planes. Factors affecting these errors were discussed; specifically the calibration methods used to align IMMSs to body segments and the inevitable STA. Nevertheless, it is shown that the hip joint angle accuracy in the sagittal and coronal planes is sufficient to be used for biomechanical studies. Future work will expand the Pendulum Filter to a full lower body model.

References

[1] S. A. Jobson, A. M. Nevill, S. R. George, A. E. Jeukendrup, and L. Passfield, "Influence of body position when considering the ecological validity of laboratory time-trial cycling performance," *J. Sports Sci.*, vol. 26, no. 12, pp. 1269–1278, 2008.

[2] S. A. Jobson, A. M. Nevill, G. S. Palmer, A. E. Jeukendrup, M. Doherty, and G. Atkinson, "The ecological validity of laboratory cycling: Does body size explain the difference between laboratory- and field-based cycling performance?" *J. Sports Sci.*, vol. 1, no. 25, pp. 3–9, 2007.

[3] A. Jones and J. Doust, "A 1% treadmill grade most accurately reflects the energetic cost of outdoor running," *J. Sports Sci.*, vol. 14, no. 4, pp. 321–327, 1996.

[4] K. Baert *et al.*, "Technologies for highly miniaturized autonomous sensor networks," *Microelectron. J.*, vol. 37, no. 12, pp. 1563–1568, 2006.

[5] D. Gouwanda and S. M. N. A. Senanayake, "Emerging trends of body-mounted sensors in sports and human gait analysis," in *Proc. 4th Kuala Lumpur Int. Conf. Biomed. Eng., 2008*, Kuala Lumpur, Malaysia, pp. 715–718.

[6] D. Roetenberg, "Inertial and magnetic sensing of human motion," Ph.D. dissertation, Biomedical Technology Inst., Univ. Twente, Enschede, The Netherlands, 2006.

[7] C. Verplaetse, "Inertial proprioceptive devices: Self-motion-sensing toys and tools," *IBM Syst. J.*, vol. 35, nos. 3–4, pp. 639–650, 1996.

[8] E. Foxlin, "Motion tracking requirements and technologies," in *Handbook of Virtual Environment Technology*. Mahwah, NJ, USA: Lawrence Erlbaum Assoc., 2002, ch. 8, pp. 163–210.

[9] D. Roetenberg, H. Luinge, and P. Slycke. (2009, Apr.). *Xsens Homepage* [Online]. http://www.xsens.com/images/stories/PDF/MVN_white_paper.pdf

[10] R. Harle, "A survey of indoor inertial positioning systems for pedestrians," *IEEE Commun. Surv. Tuts.*, vol. 15, no. 3, pp. 1281–1293, Jul. 2013.
[11] A. Cutti, A. Ferrari, P. Garofalo, M. Raggi, A. Cappello, and A. Ferrari, "'Outwalk': A protocol for clinical gait analysis based on inertial and magnetic sensors," *Med. Biol. Eng. Comput.*, vol. 48, no. 1, pp. 17–25, 2010.
[12] K. Altun, B. Barshan, and O. Tunçel, "Comparative study on classifying human activities with miniature inertial and magnetic sensors," *Pattern Recognit.*, vol. 43, no. 10, pp. 3605–3620, 2010.
[13] H. Zhou and H. Hu, "Human motion tracking for rehabilitation—A survey," *Biomed. Signal Process. Control*, vol. 3, no. 1, pp. 1–18, 2008.
[14] O. J. Woodman, "An introduction to inertial navigation," Comput. Lab., Univ. Cambridge, Cambridge, U.K., Tech. Rep. 696, 2007.
[15] A. M. Sabatini, "Estimating three-dimensional orientation of human body parts by inertial/magnetic sensing," *Sensors*, vol. 11, no. 2, pp. 1489–1525, 2011.
[16] J. L. Crassidis, F. L. Markley, and Y. Cheng, "Survey of nonlinear attitude estimation methods," *J. Guid., Control, Dyn.*, vol. 30, no. 1, pp. 12–28, 2007.
[17] D. Simon, "A comparison of filtering approaches for aircraft engine health estimation," *Aerosp. Sci. Technol.*, vol. 12, no. 4, pp. 276–284, 2008.
[18] W. T. Higgins, "A comparison of complementary and Kalman filtering," *IEEE Trans. Aerosp. Electron. Syst.*, vol. AES-11, no. 3, pp. 321–325, May 1975.
[19] M. D. Hua, G. Ducard, T. Hamel, R. Mahony, and K. Rudin, "Implementation of a nonlinear attitude estimator for aerial robotic vehicles," *IEEE Trans. Control Syst. Technol.*, vol. 22, no. 1, pp. 201–213, Jan. 2014.
[20] R. Mahony, T. Hamel, and J. M. Pflimlin, "Nonlinear complementary filters on the special orthogonal group," *IEEE Trans. Autom. Control*, vol. 53, no. 5, pp. 1203–1218, Jun. 2008.
[21] X. N. Y. L. Q. Zhang, Y. Cheng, and C. Shi, "Observability analysis of non-holonomic constraints for land-vehicle navigation systems," *J. Global Position. Syst.*, vol. 11, no. 1, pp. 80–88, 2012.
[22] J. Pusa, "Strapdown inertial navigation system aiding with nonholonomic constraints using indirect Kalman filtering," M.S. thesis, Dept. Math., Faculty of Science and Environmental Engineering, Tampere Univ. Technol., Tampere, Finland, 2009.
[23] H. J. Luinge, P. H. Veltink, and C. T. M. Baten, "Ambulatory measurement of arm orientation," *J. Biomech.*, vol. 40, no. 1, pp. 78–85, 2007.
[24] V. T. van Hees *et al.*, "Separating movement and gravity components in an acceleration signal and implications for the assessment of human daily physical activity," *PLOS ONE*, vol. 8, no. 4, p. e61691, 2013.
[25] H. J. Luinge and P. H. Veltink, "Inclination measurement of human movement using a 3-D accelerometer with autocalibration," *IEEE Trans. Neural Syst. Rehabil. Eng.*, vol. 12, no. 1, pp. 112–121, Mar. 2004.
[26] R. Mahony, M. K. J. Euston, P. Coote, and T. Hamel, "A non-linear observer for attitude estimation of a fixed-wing unmanned aerial vehicle without GPS measurements," *Trans. Inst. Meas. Control*, vol. 33, no. 6, pp. 699–717, 2011.
[27] H. J. Luinge and P. H. Veltink, "Measuring orientation of human body segments using miniature gyroscopes and accelerometers," *Med. Biol. Eng. Comput.*, vol. 43, no. 2, pp. 273–282, 2005.
[28] P. Rizun, "Optimal Wiener filter for a body mounted inertial attitude sensor," *J. Navigat.*, vol. 61, no. 3, pp. 455–472, 2008.
[29] J. K. Lee, E. J. Park, and S. N. Robinovitch, "Estimation of attitude and external acceleration using inertial sensor measurement during various dynamic conditions," *IEEE Trans. Instrum. Meas.*, vol. 61, no. 8, pp. 2262–2273, Aug. 2012.
[30] J. Cockcroft, "An evaluation of inertial motion capture technology for use in the analysis and optimization of road cycling kinematics," M.S. thesis, Dept. Mech. Mechatronic Eng., Stellenbosch Univ., Stellenbosch, South Africa, 2011.
[31] S. J. Cockcroft and C. Scheffer, "Determining the feasibility of measuring outdoor road cycling kinematics using inertial motion capture technology," *SAIEE Africa Res. J.*, vol. 102, no. 1, pp. 31–39, 2011.
[32] R. Marin-Perianu *et al.*, "A performance analysis of a wireless body-area network monitoring system for professional cycling," *Personal Ubiquitous Comput.*, vol. 17, no. 1, pp. 197–209, 2013.
[33] W. H. K. De Vries, H. E. J. Veeger, C. T. M. Baten, and F. C. T. Van Der Helm, "Magnetic distortion in motion labs, implications for validating inertial magnetic sensors," *Gait Posture*, vol. 29, no. 4, pp. 535–541, 2009.
[34] Y. Xiaoping, E. R. Bachmann, and R. B. McGhee, "A simplified quaternion-based algorithm for orientation estimation from earth gravity and magnetic field measurements," *IEEE Trans. Instrum. Meas.*, vol. 57, no. 3, pp. 638–650, Mar. 2008.
[35] T. Cloete and C. Scheffer, "Benchmarking of a full-body inertial motion capture system for clinical gait analysis," in *Proc. 30th Annu. Int. Conf. IEEE EMBS*, Aug. 2008, pp. 4579–4582.
[36] H. Zhou and H. Hu, "Reducing drifts in the inertial measurements of wrist and elbow positions," *IEEE Trans. Instrum. Meas.*, vol. 59, no. 3, pp. 575–585, Mar. 2010.
[37] S. Zhang, H. Hu, and H. Zhou, "An interactive Internet-based system for tracking upper limb motion in home-based rehabilitation," *Med. Biol. Eng. Comput.*, vol. 46, no. 3, pp. 241–249, 2008.
[38] H. Zhou, T. Stone, H. Hu, and N. Harris, "Use of multiple wearable inertial sensors in upper limb motion tracking," *Med. Eng. Phys.*, vol. 30, no. 1, pp. 123–133, 2008.

John Cockcroft is currently pursuing the Ph.D. degree in engineering at the Stellenbosch University, Matieland, South Africa. He received the M.Sc. degree in engineering in 2011, focusing on the use of inertial sensors for analyzing road cycling biomechanics. He is also currently working as the Manager and Motion Analysis Engineer with the Biomechanics Laboratory, Stellenbosch University.

Jacobus H. Muller received the Ph.D. degree in engineering from Stellenbosch University, in 2010, where he is currently a Senior Lecturer with the Department of Mechanical and Mechatronic Engineering. His current primary research interests include computational biomechanics and musculoskeletal modelling.

Corie Scheffer received the Ph.D. degree in engineering from the University of Pretoria, in 2002, where he was a Research Fellow with the Dynamic Systems Group from 1998 to 2002. He has been with the Department of Mechanical and Mechatronic Engineering, Stellenbosch University, since 2004, and he is the Founder and Head of the Biomedical Engineering Research Group.